Investigation of Chemical and Thermal Stability of Li7–xLa3Zr2–xTaxO12 Garnet Type Solid-State Electrolyte to Assemble Self-Standing Li-based All Solid-State Battery

Ghassen Charrad, Sarah Pradeilles, Romain Berthelot, P.-L. Taberna, Patrice Simon, Patrick Rozier

HAL Id: hal-04119284
https://hal.science/hal-04119284

Submitted on 6 Jun 2023

Investigation of Chemical and Thermal Stability of Li$_{7-x}$La$_3$Zr$_{2-x}$Ta$_x$O$_{12}$ Garnet Type Solid-State Electrolyte to Assemble Self-Standing Li-based All Solid-State Battery

*Ghassen Charrad, Sarah Pradeilles, Romain Berthelot, Pierre-Louis Taberna, Patrice Simon, and Patrick Rozier**

All solid-state batteries (ASSB) are the next generation of safe and high-energy-density energy storage technology. Their development is currently impeded by the stability issues of solid-state electrolyte (SSE) limiting the creation of interfaces of quality high enough to ensure efficient transfer of charges. The garnet Li$_{7-x}$La$_3$Zr$_{2-x}$Ta$_x$O$_{12}$ (LLZO:Ta) is one of the most appealing oxide-based SSE but its high sensitivity to moist air engenders difficulties in designing process to densify and assemble components of the ASSB. Based on a careful investigation of LLZO:Ta thermal and chemical stability, a heat treatment is designed and shown to fully reverse the protonation process. The investigation of spark plasma sintering protocols confirms that pretreated LLZO:Ta can be densified at a temperature as low as 850 °C or with a short duration (few seconds) at 900 °C. The characterization of obtained ceramics shows conductivities close to the bulk properties and confirms the absence of influence of grain boundaries. The study of composite electrodes shows that LLZO:Ta is suitable to act both as SSE separator and ionic percolator in positive electrode, the selection of active material remains the main issue to target self-standing Li-based ASSB.

G. Charrad, S. Pradeilles, P.-L. Taberna, P. Simon, P. Rozier
Université Toulouse III Paul Sabatier
CIRIMAT UMR CNRS 5085
31062 Toulouse, France
E-mail: patrick.rozier@univ-tlse3.fr

G. Charrad, R. Berthelot, P.-L. Taberna, P. Simon, P. Rozier
CNRS
Réseau sur le Stockage Electrochimique de l'Energie (RS2E)
80000 Amiens, France

S. Pradeilles
Saint Gobain Research Provence
84300 Cavaillon, France

R. Berthelot
ICGM
Université Montpellier
CNRS
ENSCM
34000 Montpellier, France

The ORCID identification number(s) for the author(s) of this article can be found under https://doi.org/10.1002/ente.202300234.

1. Introduction

All solid-state batteries (ASSB) in which a solid-state electrolyte (SSE) replaces the liquid one used in commercialized Li-ion batteries are the most promising technology to reach safe and high energy system to power electric vehicles. The use of SSE, which are nonflammable, prevents all safety issues associated with the use of organic and flammable liquid electrolytes. In addition, dense SSE acts as a mechanical barrier to the growth of Li dendrite preventing internal short-circuit thus allowing the use of high-capacity metallic lithium anode electrode toward high energy density batteries.[1,2] The main drawback of using an SSE is the need of a specific process to create and maintain along cycling solid/solid interfaces of quality high enough to ensure an efficient transport of charge carriers. Mainly two classes of SSE are currently under investigation and their characteristics govern the process to be optimized. For example, sulfide-based SSEs like argyrodite are soft materials with high malleability implying that simple compaction at room temperature ensures good charges transport but, as a main drawback, that this pressure should be maintained during the working of the cell.[3,4] In a fully opposite way, oxide-based SSEs such as garnet Li$_7$La$_3$Zr$_2$O$_{12}$ are hard material with low malleability implying that a sintering process often occurring at high temperatures is needed to create the interfaces. However, once created, the interfaces are maintained at room temperature without the need of high external pressure. While such self-standing systems offer clear advantages in terms of packaging, the needed high-temperature sintering process exacerbates all phenomena such as grain growth, structure changes, or reactive processes in composites or during the assembling of multi-materials. The central component of ASSB is the SSE, its selection should be made based on its ionic conductivity and on its thermal and chemical stabilities toward the other components such as metallic Li, positive electrode active material, and possibly other additive such as electronic conductors. Among the different classes of oxide-based SSE, the garnet Li$_7$La$_3$Zr$_2$O$_{12}$ has attracted interest due to the high ionic conductivity of the cubic polymorph, chemical stability against metallic lithium, and large electrochemical stability window.[5,6] More precisely,

the aliovalent substitution of Ta^{5+} for Zr^{4+} allows stabilizing at room temperature the conductive cubic polymorph and creating Li^+ vacancies leading to the highest ionic conductivity of 10^{-3} S cm^{-1} at room temperature for $Li_{7-x}La_3Zr_{2-x}Ta_xO_{12}$ (LLZO:Ta) with $0.5 \leq x \leq 0.6$.[7–9] Nevertheless, two main drawbacks of LLZO:Ta have been identified. The first one corresponds to the need of controlling multiple parameters of the synthesis process (atmosphere, nature of sample holder, annealing temperature, ...) all affecting largely the properties. The second one is the high sensitivity of LLZO:Ta to moist air which provokes the Li^+/H^+ exchange resulting in a mixture of $Li_{6.5-x}H_xLa_3Zr_{1.5}Ta_{0.5}O_{12}$ (HLZO:Ta) protonated phase with LiOH and Li_2CO_3 side products. The easy obtaining of an insulating protonated phase with a variable amount of side products leads to a drastic change in the behavior of LLZO:Ta during sintering process and drastic change of the physical properties of the obtained ceramic. The combination of the influence of synthesis parameters and sensitivity to moist air explains the discrepancies of reported results regarding shaping process, ionic conductivity of ceramics as well as (electro-)chemical stability against active materials such as $Li[Ni,Mn,Co]O_2$ (NMC) layered oxides.[10–12] While the origin of such discrepancies is well-known and frequently used to explain difficulties in getting reproducible results, the precise influence of moisture sensitivity and how to balance it has not been clearly investigated.

In this report, we analyze the thermal and chemical stability of LLZO:Ta and propose a pretreatment protocol of the powdered sample designed to fully reverse the reaction with moist air. Following that, we are able to design a process, using spark plasma sintering (SPS) technique, and to determine the range of parameters (temperature, heating rate, and pressure) to obtain dense single-phase cubic polymorph of fully lithiated LLZO:Ta with optimal transport properties. In addition, we report the investigation of the chemical stability of pretreated LLZO:Ta with active materials (AM) and demonstrate that the limiting factor to the obtaining of dense composite electrode material is the stability of the AM. We show that SPS parameters can be optimized to obtain a relatively dense LLZO:Ta/AM composite while the reactivity of selected AM with carbon commonly used electronic additive prevent for obtaining the complete composite electrode.

2. Results and Discussion

2.1. Chemical and Thermal Stability of LLZO:Ta

The pristine LLZO:Ta is analyzed to determine initial characteristics. ICP-AES (**Table 1**) leads to a chemical composition "$Li_{7.05}La_3Zr_{1.40}Ta_{0.58}O_{12}$" instead of "$Li_{6.4}La_3Zr_{1.4}Ta_{0.6}O_{12}$" showing, besides a good agreement for La/Zr/Ta ratio, a Li content larger than requested to balance the electroneutrality of the sample indicating the presence of Li-based side products. The X-ray diffraction pattern (**Figure 1**a) confirms that the sample is a mixture of the cubic–LLZO structure (space group Ia–$3d$) and Li_2CO_3 identified by the presence of the (110) peak at $2\theta = 21.42°$.[10,13] The refined, using profile matching method,[14] lattice parameter $a = 13.035(3)$ Å, higher than that reported for LLZO:Ta ($a = 12.95$ Å),[15] is close to the one ($a = 13.0123$ Å) of protonated $Li_{6.5-x}H_xLa_3Zr_{1.5}Ta_{0.5}O_{12}$ compound (HLZO:Ta).[16] The SEM

Table 1. ICP-AES results and atomic composition normalized to La content for the pristine powder LLZO:Ta and water-treated LLZO:Ta–H_2O.

Sample	Li	La	Zr	Ta
Pristine LLZO:Ta		Element in ppm		
	34.46	293	89.98	59.21
		Normalized to La		
	7.10(6)	3	1.40(8)	0.58(7)
LLZO:Ta-H_2O		Element in ppm		
	28.7	1186	364.41	258.6
		Normalized to La		
	1.45(6)	3	1.40(5)	0.49(9)
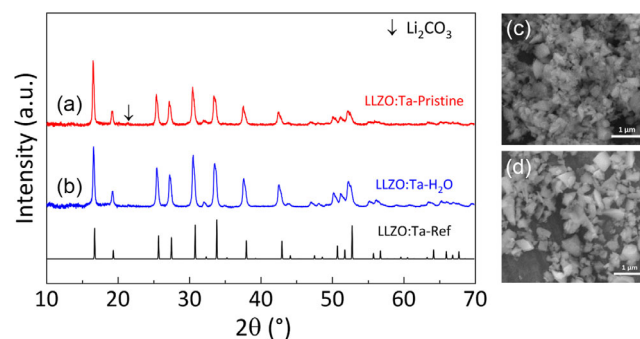
Figure 1. XRD patterns of a) pristine LLZO:Ta and b) water-treated LLZO:Ta–H_2O compared to the reference pattern of LLZO:Ta. SEM images of c) pristine LLZO:Ta and d) water-treated LLZO:Ta–H_2O.

images (Figure 1c) show irregular shapes of particles with the presence of many agglomerates and additional small-sized particles. The particle size distribution determined using laser diffraction analysis shows that the D_{10}, D_{50}, and D_{90} are 0.355, 0.753, and 2.635 µm respectively. XPS experiments have been conducted and the examination of the O $1s$ spectra (Figure S1, Supporting Information) shows three peaks at 532, 531, and 529 eV that are assigned respectively to Li_2CO_3, LiOH, and to the oxygen in the lattice of LLZO:Ta.[17]

The combination of all the characterization techniques confirms that the pristine LLZO:Ta sample corresponds to a mixture of at least partially protonated cubic garnet with estimated composition $Li_{6.4-x}H_xLa_3Zr_{1.4}Ta_{0.58}O_{12}$ (denoted as HLZO:Ta), Li_2CO_3 as deduced from XRD and confirmed using XPS and also LiOH which cannot be observed in the XRD pattern but has been detected using XPS analysis. While the as-received sample has been handled and stored in the glove box, the presence of protonated phase and side products underlines the high moisture sensitivity of LLZO:Ta. To investigate deeper this sensitivity, a part of the sample has been left in the air for a week, and another part soaked in water. The analysis of the air-aged sample shows that while no clear change on the XRD pattern or SEM images can be detected, XPS C $1s$ and O$1s$ spectra show a larger amount of Li_2CO_3 than for the pristine LLZO:Ta (Figure S1, Supporting Information). This indicates that the reaction with moist air follows first

$$Li_{6.4}La_3Zr_{1.4}Ta_{0.6}O_{12} + H_2O \rightarrow Li_{6.4-x}H_xLa_3Zr_{1.4}Ta_{0.6}O_{12} + xLiOH$$

ADVANCED
SCIENCE NEWS
www.advancedsciencenews.com

Energy Technology
Generation, Conversion, Storage, Distribution
www.entechnol.de

and that the as-produced LiOH further reacts with CO_2 in a second step to generate Li_2CO_3.[11] The evolution of the pH monitored during the immersion of the pristine LLZO:Ta in water shows that the pH increases immediately after soaking indicating a fast kinetic of the reaction in accordance with the high sensitivity of LLZO:Ta. The soaked sample has been filtered, rinsed in water, and dried at 60 °C under vacuum to remove adsorbed water. The XRD analysis of the sample shows that it corresponds to single-phase cubic garnet type (Figure 1b) with refined cell parameters of $a = 13.028(1)$ Å characteristic of the protonated phase.[16] The ICP analysis (Table 1) confirms a small amount of remaining Li while the La/Zr/Ta ratio remains identical to one of the pristine materials. The comparison of the SEM images (Figure 1d) with that of pristine LLZO:Ta shows that only large particles are observed indicating that the smallest ones observed in pristine LLZO:Ta correspond to highly soluble side products LiOH, Li_2CO_3.

The thermal stability of the pristine LLZO:Ta is monitored using operando XRD up to 1100 °C. The evolution of the XRD patterns reported in **Figure 2**a shows, besides the sharpening of the Bragg peaks, a progressive shift of their location and the appearance and disappearance in the [500–800 °C] temperature range of a new set of Bragg peaks. The most intense peak at $2\theta = 28°$, is assigned to $La_2Zr_2O_7$ already reported as the main compound obtained during the thermal decomposition of protonated garnet phase.[15] At high temperature the XRD pattern is characteristic of single-phase cubic LLZO:Ta which is maintained after cooling down back to room temperature. The evolution of refined cell parameter reported in the Figure 2b shows that from RT to 600 °C a value of $a = 13.03$ Å is maintained followed by a linear increase up to $a = 13.17$ Å at 1100 °C. After cooling down to room temperature, the refined lattice parameter $a = 12.95$ Å corresponds to the one of purely lithiated LLZO:Ta compound. Interestingly, the evolution along heating indicates that the H^+ to Li^+ exchange is reversed by a simple heat treatment which, based on the observation of the evolution of XRD patterns, can be dissociated into two stages depending on the

temperature. Using the melting temperature of LiOH (380 °C) and of Li_2CO_3 (850 °C) as an indirect probe of their chemical reactivity, can be proposed a mechanism explaining the two stages of the deprotonation process. At low temperatures, the reaction of HLZO:Ta with LiOH (lowest melting T so highest reactivity) is responsible for the deprotonation of HLZO:Ta. This Li^+ to H^+ replacement induces a decrease of the lattice parameter which is balanced by the lattice thermal expansion, leading to an almost constant value as observed up to 600 °C. At this temperature, the remaining protonated HLZO:Ta is not stable and decomposes as indicated by the growth of the Bragg peaks characteristic of $La_2Zr_2O_7$, while the cell parameter of LLZO:Ta increases due to thermal lattice expansion. Above 700 °C, Li_2CO_3 becomes "chemically active" and reacts with $La_2Zr_2O_7$, as confirmed by the disappearance of corresponding Bragg peaks, to form extra LLZO:Ta. Above 800 °C single-phased and purely lithiated LLZO:Ta is obtained and the evolution of cell parameters follows the lattice thermal expansion.

To confirm the results obtained using operando XRD, a batch of pristine LLZO:Ta is heated under a flow of dried argon up to 800 °C for 4h. The XRD pattern of as obtained powder (Figure S2, Supporting Information) and refined cell parameter ($a = 12.94(8)$ Å) confirm that the sample corresponds to fully lithiated LLZO:Ta. This allows concluding that despite high-moisture sensitivity of garnet structure, a simple heat treatment allows reversing the process and obtaining single-phased LLZO:Ta. However, the presence of LiOH and Li_2CO_3 as side products with different kinetics of reaction, implies that the heat treatment should be performed at a temperature above 800 °C needed to activate the reactivity of Li_2CO_3. In addition, to prevent any risk of partial protonation during the cooling of the sample, heat treatment should be performed under a dry atmosphere.

Knowing that for ASSB, the electrolyte should also be used as ionic percolator in the positive electrode composite, we decided to investigate the stability of a LLZO:Ta/NMC811 mixture. The latter has been selected because it is one of the most promising candidates to be used in ASSB technologies and is widely used in
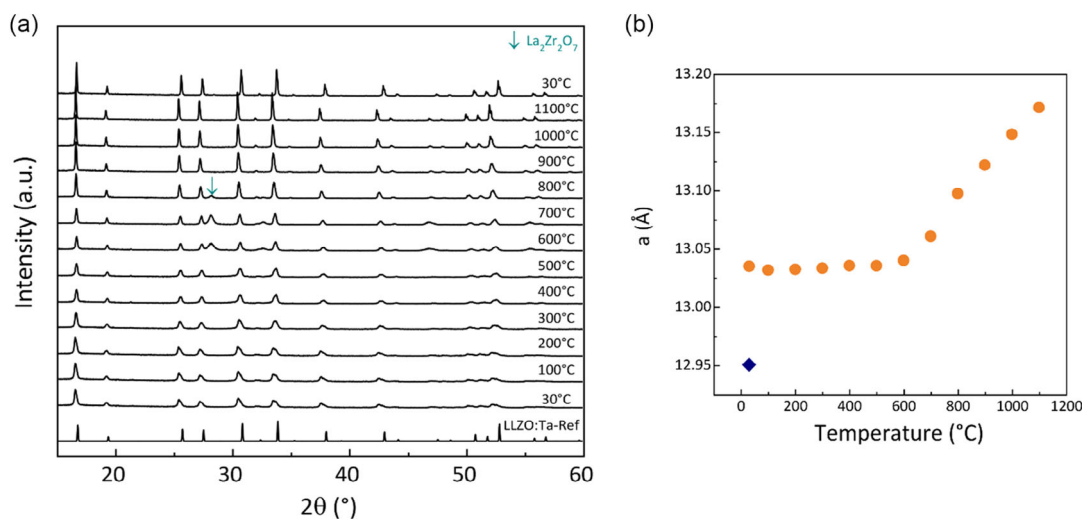
Figure 2. a) XRD patterns collected operando during the heating of pristine LLZO:Ta and compared with calculated patterns of LLZO:Ta and $La_2Zr_2O_7$ b) Evolution of refined lattice parameter of garnet structure as a function of temperature.

**ADVANCED
SCIENCE NEWS**
www.advancedsciencenews.com

Energy Technology
Generation, Conversion, Storage, Distribution
www.entechnol.de

commercial Li-ion liquid-based batteries. The stability of the mixture is monitored using operando XRD during the heating of 30/70 vol% mixture of pretreated LLZO:Ta-Ar/NMC811 in air. The comparison of the XRD patterns reported in **Figure 3**a shows, besides, the shift of Bragg peaks of both compounds, above 700 °C, the progressive disappearance of (00l) Bragg peaks of NMC. Upon cooling back to room temperature, LLZO:Ta is maintained, and broad (00L) Bragg peaks of layered NMC are restored.

The evolution of the refined cell parameters of the garnet structure (Figure 3b) shows a large increase up to 100 °C which can be explained by the formation of protonated HLZO:Ta in agreement with sensitivity of LLZO:Ta with moist air. Above 100 °C, the cell parameter remains constant indicating the occurrence of the reverse reaction (deprotonation) which is completed at 400 °C above which cell parameter evolution follows thermal lattice expansion. The completeness of the reaction at low temperature confirms that LiOH is the only side product and that at high-temperature deprotonation is favored compared to the carbonation of LiOH.

These observations allow concluding that besides the thermal stability of partially protonated HLZO:Ta described in the first part, no extra evolution of the LLZO:Ta compound is evidenced thus confirming that it is stable against NMC811. However, the evolution of the NMC diffraction pattern clearly shows that NMC 811 undergoes some structure changes at high temperature. Even if these structural changes are reversible, they should be kinetically limited as the fast cooling rate used during operando XRD experiment prevent the full recovery of sharp Bragg peaks of layered NMC.

The monitoring of the thermal and chemical stability of LLZO:Ta against moisture and active material allows concluding that while LLZO:Ta and NMC appear stable, they, in fact, undergo reactions occurring in a wide temperature range (low and high temperatures for, respectively, deprotonation of LLZO:Ta and structure changes for NMC) that should be taken into account for designing the sintering processes.
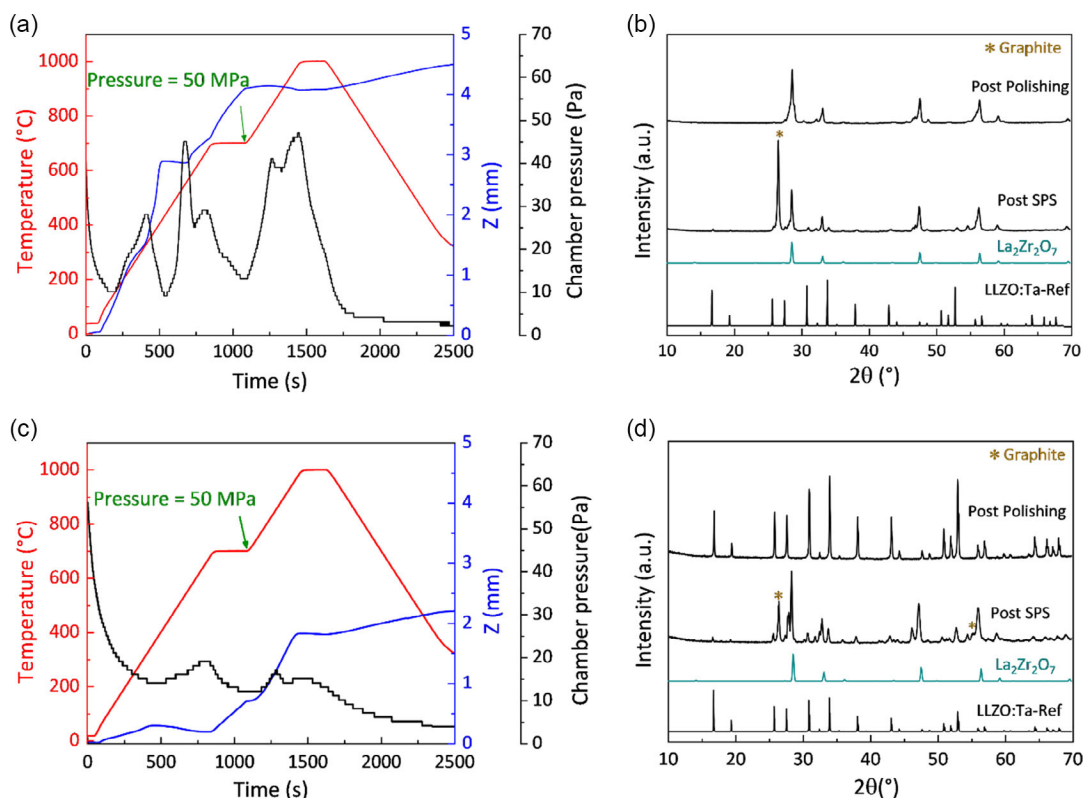
2.2. Sintering/Densification of LLZO:Ta

Among the different densification/sintering techniques, we decided to use spark plasma sintering (SPS) also known as field-assisted sintering techniques. This technique is characterized by the combination of applied uniaxial pressure and the use of high-intensity current through the punches and mold to heat the sample. It allows fast sintering of compounds at lower temperatures than conventional ones and does not require the use of sintering additive avoiding the risk of extra chemical instability. Moreover, the monitoring of the displacement of punches and the evolution of the pressure in the SPS chamber allow to collect operando, information on the densification stage and degassing phenomena. To allow a direct comparison of results, all samples have been prepared the same way as described in the experimental part.

A first test is made using the pristine LLZO:Ta and applying a constant heating rate of 50 °C min^{-1} up to 1000 °C and a constant pressure of 50 MPa. The result (not shown) indicates a huge increase in the pressure in the chamber as soon as the temperature increases associated with powder forced out of the mold. This shows that a high heating rate and, even if moderate, pressure do not allow the smooth completion of the different chemical processes corresponding to the deprotonation of pristine LLZO:Ta. The sintering parameters are then adapted to take into account these processes. As depicted in the **Figure 4**a, the initial pressure is lowered down to 10 MPa, the lowest pressure needed to maintain electrical contact. The temperature is increased with a heating rate of 50 °C min^{-1} up to 700 °C maintained for 3 min to allow the completion of deprotonation processes. At the end of this dwell, the pressure is increased up to 50 MPa and the temperature up to 1000 °C (heating rate of 50 °C min^{-1}) and maintained for 3 min before cooling the sample. The evolution of the pressure in the chamber (Figure 4a) shows high degassing phenomena at 200, 400, and 800 °C associated with a large increase of the punch displacement (Z) characteristic of a decrease of the sample thickness. The XRD patterns of the pellet as recovered
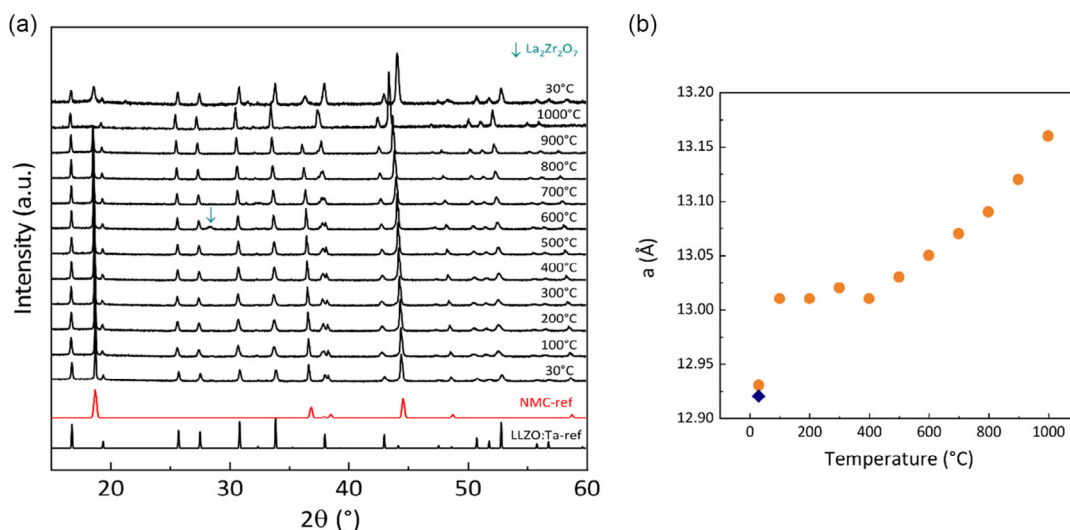
Figure 3. a) XRD patterns collected operando during the heating of the mixture LLZO:Ta + NMC811 compared with calculated patterns of LLZO:Ta and layered oxide NMC and b) evolution of LLZO:Ta refined cell parameter.

ADVANCED
SCIENCE NEWS
www.advancedsciencenews.com

Energy Technology
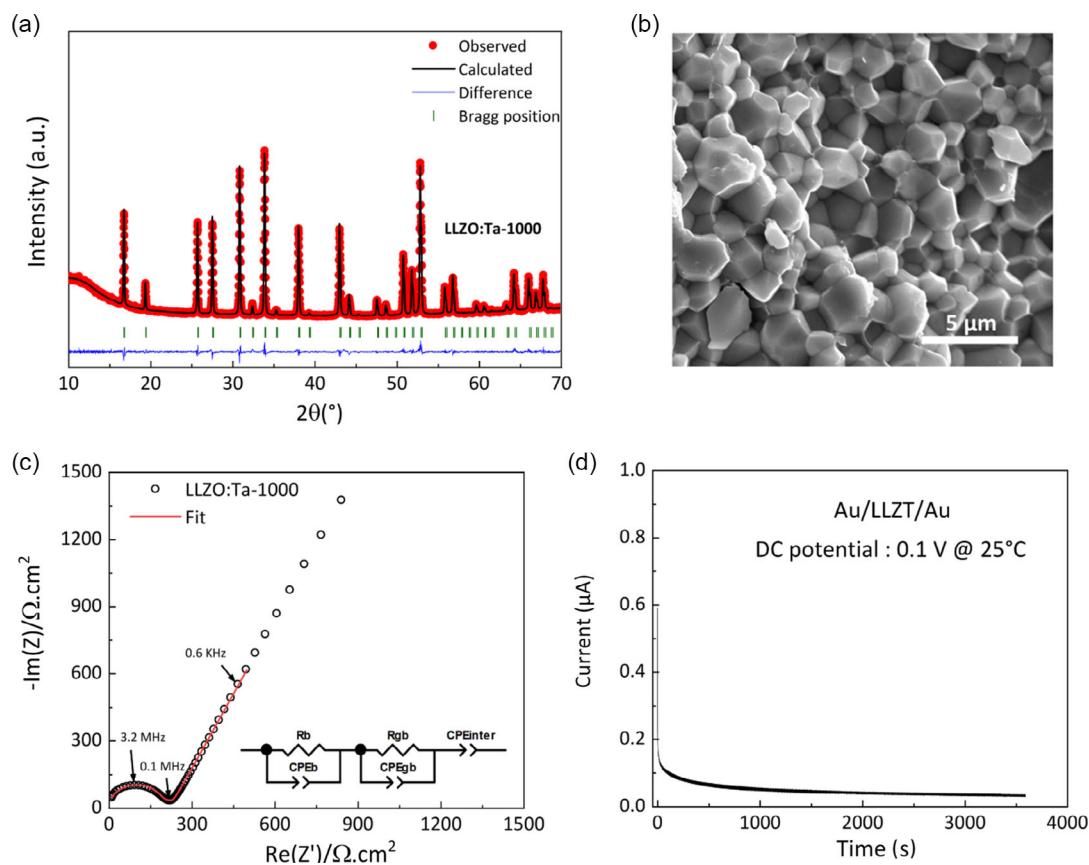Generation, Conversion, Storage, Distribution

www.entechnol.de

Figure 4. SPS protocol and collected displacement of punches and pressure of the chamber during the processing of a) the pristine LLZO:Ta powder and b) the argon-pretreated powder. Experimental XRD pattern of the densified pellet after the SPS process and after polishing compared to the calculated ones for LLZO:Ta reference and $La_2Zr_2O_7$ c) pristine LLZO:Ta powder and d) the argon pretreated powder.

and after polishing (Figure 4c), show, besides residual carbon at the surface, the presence of mainly $La_2Zr_2O_7$ without evidence of remaining LLZO:Ta. $La_2Zr_2O_7$ being the main decomposition product of protonated HLZO:Ta, obviously, the specificities of SPS treatment, such as a high heating rate, prevent the completion of the deprotonation mechanism. A batch of pristine LLZO: Ta is then pretreated at 800 °C for 4 h under a dried atmosphere (Ar) to ensure full deprotonation of the sample and used for another SPS experiment conducted while keeping the same protocol for temperature and uniaxial pressure evolutions. The evolution of the pressure in the chamber (Figure 4b) shows very low degassing phenomena in agreement with the completion of deprotonation processes during the pretreatment of the powder. The evolution of the displacement confirms the densification of the sample to occur along the heating process and to be almost finished when reaching 1000 °C as no extra evolution is observed during the dwell. The XRD patterns (Figure 4d) show that the surface of the pellet is mainly constituted of residual carbon and $La_2Zr_2O_7$ while the core of the pellet is constituted of LLZO:Ta.

To confirm the homogeneity of the sample and nature of garnet compounds, the pellet is grinded. The analysis of the XRD pattern (**Figure 5**a) of the obtained powder confirms that it is homogeneously composed of single-phased LLZO:Ta and refined cell parameter ($a = 12.935(2)$ Å) shows that fully lithiated $Li_{6.4}La_3Zr_{1.4}Ta_{0.6}O_{12}$ is obtained. The analysis of the SEM image

of a cross-section of the pellet (Figure 5b) shows grain sizes from 0.5 to 3 µm indicating a grain growth in agreement with sintering process at high temperatures but limited as usually observed with SPS process. This experiment has been repeated to ensure reproducibility leading to obtain single-phased LLZO:Ta pellets with relative density of 98% and thicknesses in a range from 0.5 to 2.5 mm.

The electrical properties of the pellet are determined at 25 °C using electrochemical impedance spectroscopy on an Au/LLZO: Ta/Au symmetrical cell. The Nyquist plot (Figure 5c) shows at high frequency, a semicircle associated with the bulk and grain boundaries resistivity followed by a fast increase of the impedance at low frequency related to the capacitive behavior of the blocking electrode. The fitting of the data using an equivalent electrical circuit leads to estimate a total ionic conductivity of $7.00(4) \times 10^{-4}$ S cm^{-1} at 25 °C close to the intrinsic bulk conductivity (3×10^{-3} S cm^{-1}) reported for LLZO:Ta.[18,19] The grain boundary conductivity $\sigma_{GB} = 5(2) \times 10^{-5}$ S cm^{-1}, estimated using Brick layer model,[20,21] confirms not only their resistive character but also their weak contribution to the total conductivity. The electronic conductivity is determined from the resistance calculated using the current I measured at the steady state (when $\frac{dI}{dt} \to 0$) after a DC voltage of 100 mV is applied (Figure 5d). A value of $\sigma_{elec} = 5.04(2) \times 10^{-8}$ S cm^{-1} is calculated which matches the intrinsic electronic conductivity of LLZO:Ta (10^{-9} S cm^{-1}).[22,23]

**ADVANCED
SCIENCE NEWS**
www.advancedsciencenews.com

Energy Technology
Generation, Conversion, Storage, Distribution

www.entechnol.de

Figure 5. a) Rietveld refinement results of the XRD pattern of the pellet sintered at 1000 °C b) Cross-section SEM image of the LLZO:Ta sintered ceramic. c) Nyquist plot for the electrochemical impedance of LLZO:Ta densified by SPS at 1000 °C placed between two Au blocking electrodes and the corresponding fit with the equivalent circuit. d) The current–time curve of the Au/LLZO:Ta/Au cell under DC polarization at different potentials.

These results demonstrate that the specificities of SPS technique, mainly high heating rate and short duration of thermal treatment, do not allow the completion of deprotonation process which should then be decoupled from the sintering process using the pretreatment under dry atmosphere designed in the previous section. Then using pretreated garnet, it is demonstrated that the SPS process allows reaching dense single-phased LLZO:Ta with ionic and electronic conductivities close to the intrinsic values indicating minimization of grain boundary contribution.
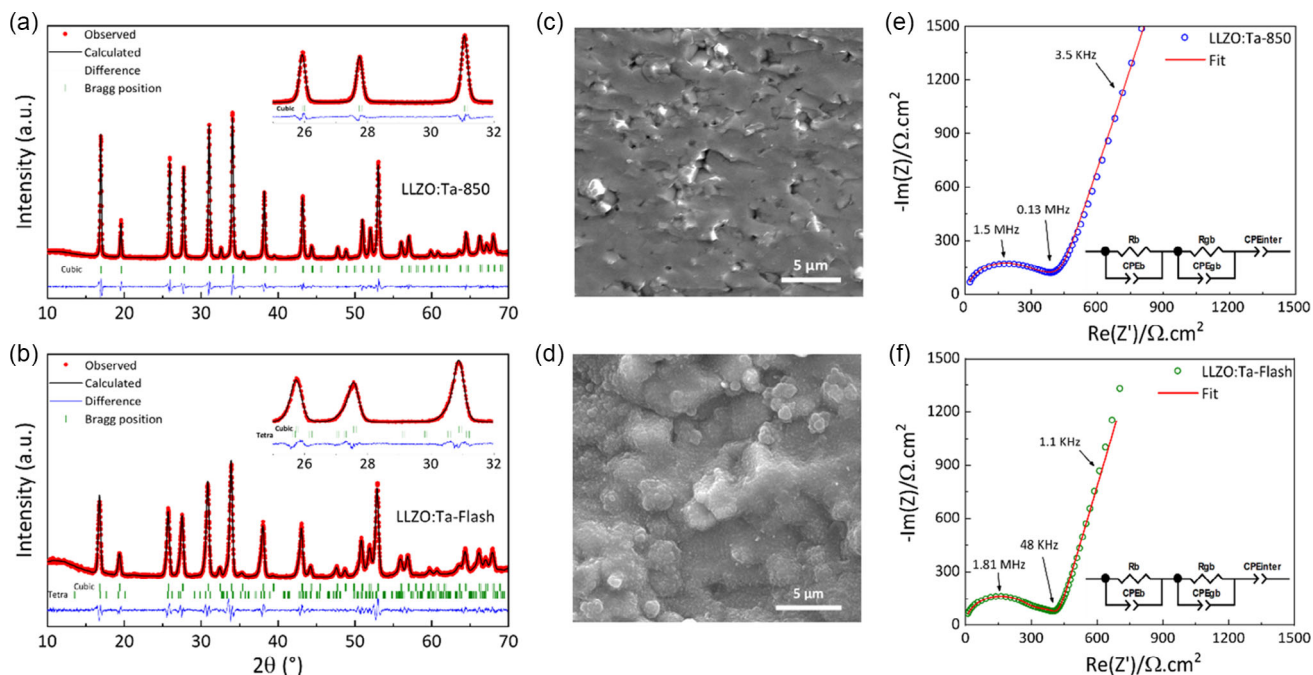
2.3. Toward Densification of Positive Electrode Composite

Once obtaining of a dense ceramic of LLZO:Ta with physical properties adequate to its use as SSE separator in ASSB is validated, the possibility to densify a composite NMC811/LLZO:Ta/C acting as positive electrode has still to be investigated. As demonstrated in the previous section, NMC811 undergoes structure changes above 700 °C which, even if reversible, may prevent the obtaining of stable interfaces of quality high enough to ensure both ionic and electronic percolation over the whole electrode. One way to solve this issue can be to decrease the sintering temperature or the duration of the dwell at high temperature compared to what is needed to fully densify single-phase LLZO:Ta. To

evaluate the temperature range and minimal dwell time at high temperatures needed to maintain both mechanical and electric properties of the SSE extra experiments have been performed on the densification of solely LLZO:Ta.

The evaluation of the effect of a decrease in the sintering temperature has been conducted using pretreated LLZO:Ta and optimized SPS protocol (Figure S3, Supporting Information) already described while limiting the sintering temperature. The characterization of the pellet densified with a sintering temperature of 850 °C shows that single-phased LLZO:Ta is obtained (**Figure 6**a). The relative density is around 95% and the total ionic conductivity of $\sigma_{ion} = 3.60(9) \times 10^{-4}$ S cm^{-1}, which, despite lowered, remains at an acceptable value for the targeted application. Different tests made with maximal sintering temperatures limited below 850 °C lead to obtain pellets with low relative density and weak mechanical strength preventing their use as mechanical separator of ASSB.

The effect of the decrease in the duration of the dwell time at high temperatures has been conducted by tuning SPS protocol to target "Flash-SPS". For this protocol (Figure S4, Supporting Information), a conventional heating rate of 50 °C min^{-1} is used up to 600 °C. This temperature, at which NMC is stable, is maintained for 20 min to allow full completion of deprotonation and residual degassing. The pressure is also progressively increased

ADVANCED
SCIENCE NEWS
www.advancedsciencenews.com

Energy Technology
Generation, Conversion, Storage, Distribution

www.entechnol.de

Figure 6. a,b) Rietveld refinement results of the XRD patterns; c,d) cross-section SEM images, and e) Nyquist plot of the impedance with the corresponding equivalent circuit, f) of respectively the LLZO:Ta pellet sintered at 850 °C and the pellet sintered using the Flash-SPS process.

up to 50 MPa. Then a direct current pulse of 720 A is applied for 15 s leading to an increase of the temperature up to 900 °C at a rate estimated around 1,500 °C min^{-1} followed by high cooling rate implying that the highest temperature is maintained for a few seconds. The relative density of the pellet is equal to 91% and the analysis of SEM image (Figure 6d) indicates particles with size in the 0.5–2 μm range, irregular shapes, and agglomerates. The XRD analysis of the pellet (Figure 6b) shows that single-phased LLZO:Ta is obtained with refined cell parameter $a = 12.923(1)$ Å in agreement with the absence of protonation, with however a clear broadening of the diffraction peaks. The broadening of the diffraction peaks, which cannot be associated with a downsizing of the particles, can be explained by the possible structure conversion from cubic to quadratic garnet type or by the presence of microstrains. The quadratic polymorph is the room-temperature stable polymorph of undoped LLZO and is considered as a distortion of the stable at high-temperature cubic polymorph. It is then expected that high heating and cooling rates may modify the relative stability of both polymorphs and allow obtaining a mixture of both polymorphs. The refined cell parameters (Figure S5, Supporting Information) considering a mixture of cubic ($a = 12.927(7)$ Å) and quadratic ($a = 13.070(5)$ Å; $c = 11.975(2)$ Å) being close to each other, the two XRD patterns overlap leading to broad diffraction peaks. The comparison of Rietveld refinement performed considering a cubic single phase or a cubic/quadratic mixture leads to better reliability factors (Figure S5, Supporting Information) for the latter but does not fully exclude the hypothesis of a high level of microstrains. The microstrains can be generated due to the high heating and cooling rate similar to quenching which does not allow the release of mechanical stress. The analysis of the evolution of

Bragg peaks full width at half maximum reported in the Williamson and Hall plot (Figure S6, Supporting Information) does not allow evidencing large microstrains while the nonmonotonous evolution is in favor of a mixture of cubic and quadratic phases. Whatever the origin of such behavior, the determination of the electrical properties shows that it has no influence on the ionic conductivity of the sample as a value of $\sigma_{ion} = 3.48(6) \times 10^{-4}$ S cm^{-1} close to the one of the samples sintered at 850 °C is obtained (Figure 6f).

The comparison of the characteristics of the pellets obtained while decreasing the sintering temperature down to 850 °C or the dwell time at high temperature down to a few seconds (**Table 2**) shows in both cases and as expected a decrease of the relative density however still above 91%. In addition, despite the ionic conductivity is lowered, the contribution of grain boundary is not clearly increased, leading to obtain ceramics with characteristics still compatible with their use as a mechanical separator for ASSB.

Based on these results, the densification of a composite including active material NMC811, LLZO:Ta as ionic percolator, and carbon as electronic percolator has been envisaged. The first tests not detailed in this report show that the well-known reduction of NMC by C electronic additive (carbo-thermal reduction process) cannot be avoided even by using a fast heating rate and short dwell time of SPS process. Trying to reduce as much as possible the duration of the high-temperature process, we applied parameters corresponding to the Flash-SPS process but in that case, also full decomposition is observed. While LLZO:Ta was confirmed to be stable in all tested configurations, the presence of carbon as electronic conductor additive is detrimental for the stability of active materials. We decided then to evaluate the stability of a LLZO:Ta/NMC composite. A mixture

ADVANCED
SCIENCE NEWS
www.advancedsciencenews.com

Energy Technology
Generation, Conversion, Storage, Distribution

www.entechnol.de

Table 2. EIS data fitting and the conductivity calculation for the obtained pellets.

	RD [%]	R_B [Ω]	σ_B [S cm^{-1}]	R_{GB} [Ω]	σ_{GB} [S cm^{-1}]	σ_{ion} [S cm^{-1}]
LLZO:Ta-1000	98(1)	212(9)	$9.30(4) \times 10^{-3}$	72(9)	$5(2) \times 10^{-5}$	$7.00(4) \times 10^{-4}$
LLZO:Ta-850	95(1)	327(7)	$6.0(1) \times 10^{-4}$	220(7)	$1.2(4) \times 10^{-4}$	$3.60(9) \times 10^{-4}$
LLZO:Ta-Flash	91(1)	346(5)	$5.5(1) \times 10^{-4}$	201(6)	$5(2) \times 10^{-5}$	$3.48(6) \times 10^{-4}$

of NMC/LLZO:Ta in an 85/15 volume ratio is ball-milled for 1 h at 400 rpm and introduced in the graphite mold. A boron nitride (BN) layer is sprayed on the surface of the carbon disks to avoid direct contact of the mixture with carbon. The SPS protocol has been tuned to take into account the limited stability of NMC811 (**Figure 7**a). A low pressure of 10 MPa is applied during the heating at a rate of 50 °C min^{-1} up to 300 °C maintained. At this temperature, a dwell time of 5 min is used to progressively increase the pressure up to 100 MPa, twice the pressure used in previous experiments to compensate for the lowering of the sintering temperature. The temperature is then increased (heating rate 50 °C min^{-1}) up to only 600 °C (stability domain of NMC811) and maintained for 10 min. The analysis of the monitored parameters during the SPS process (Figure 7a) shows that the pressure in the chamber remains constant during the whole process showing the absence of degassing phenomena. Along the dwell at 300 °C, the displacement increases drastically in agreement with the compaction of the powder due to the increase of the pressure. Along the dwell at 600 °C another increase in the displacement suggests, despite a low temperature, the beginning of the densification process. The characterization of the pellet shows that the densification process is only partial as the relative density is equal to 81%. The XRD pattern of the polished pellet (Figure 7b) confirms the absence of reactive process as only Bragg peaks of LLZO:Ta and NMC811 components are identified. The SEM images of a cross-section of the pellet show the presence of residual porosity in agreement with the low relative density and that the microstructure of pristine NMC (Figure S7, Supporting Information) and LLZO:Ta are retained in accordance with the low temperature and short duration time of the sintering process. The electrical behavior evaluated using EIS of a symmetrical Au/composite/Au cell confirms that despite ionic percolation is reached, the absence of carbon additive leads to very low electronic conductivity.

Considering the combination of these results, despite low relative density, the mechanical cohesiveness of the composite is maintained, and created interfaces are of quality high enough to ensure the ionic conduction. Opposite to the needed high-relative
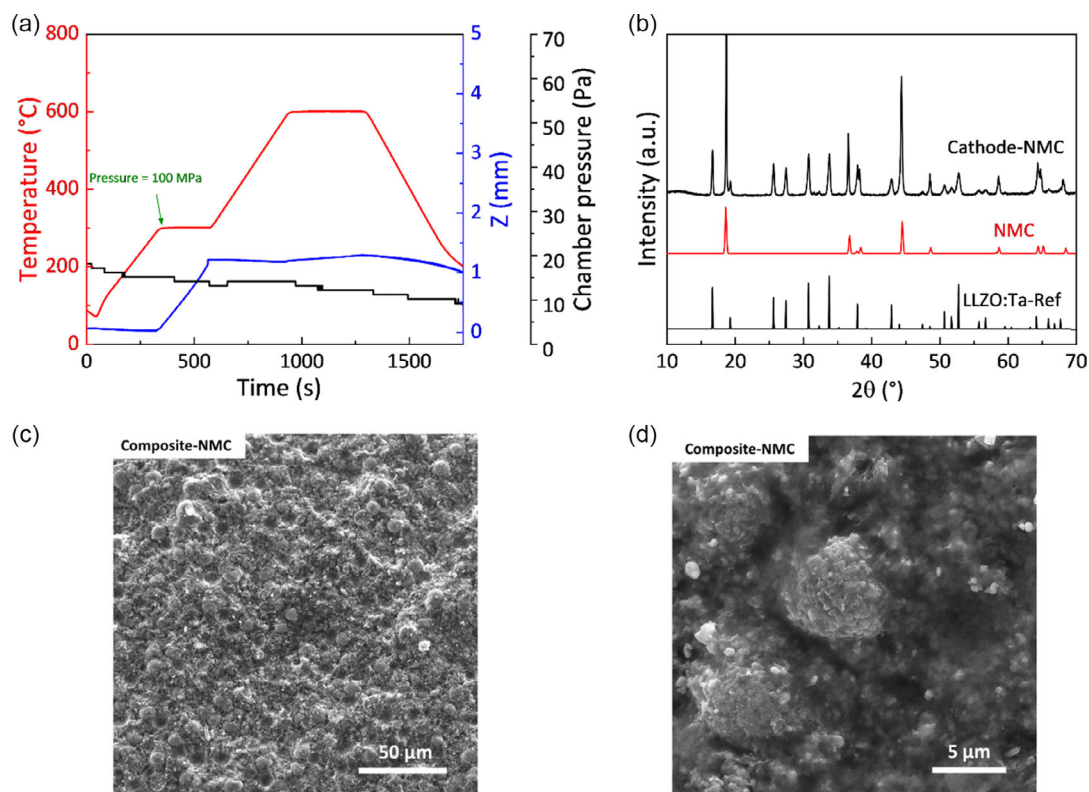
Figure 7. a) Evolution of the SPS parameters during the SPS densification of the composite cathode with NMC-811. b) XRD pattern and c,d) SEM images of the pellet composite cathode NMC postpolishing.

density of the SSE acting as a mechanical barrier to separate electrodes and prevent lithium dendrite growth, residual porosity in the composite electrode as soon as the ionic percolation is ensured, may not be an issue. It can buffer the mechanical strains induced by the volume changes of the active materials during deinsertion/insertion of Li well-known to induce contact loss or even fracturing of electrode responsible for the poor cycle life of self-standing ASSB. The optimization of the amount of residual porosity to act as a mechanical buffer without compromising the transport properties (notably polarization of the cell) will have to be investigated. The remaining issue to be solved is to reach electronic percolation but, as demonstrated, LLZO:Ta being chemically and thermally stable, it is the stability of the active material and electronic additive which are the limiting parameters.

3. Conclusion

The study of the chemical and thermal stability of a commercial LLZO:Ta garnet type SSE confirms its high moisture sensitivity and clarifies the two stages process with first the Li^+/H^+ exchange associated to the formation of LiOH which further reacts to form Li_2CO_3. It is also demonstrated that it is the presence of such mixture which prevents easy densification process and low reproducibility of results. To solve these issues, a simple heat treatment in a dry atmosphere at a temperature of 800 °C is designed allowing to fully reverse the reaction and obtain single phase fully lithiated LLZO:Ta easily densified at 1000 °C in 10 min using SPS. The characterization of the pellets shows that transport properties are comparable to reported ones for bulk LLZO:Ta confirming the absence of detrimental contribution at the grain boundaries. The study of the thermal behavior of a mixture of pretreated-LLZO:Ta with NMC active material shows that while both compounds are chemically stable, NMC undergoes structure changes at high temperature which, even if reversible, affect the sintering process. Moreover, the study of the thermal behavior of a LLZO;Ta/NMC/C mixture shows that NMC is fully reduced by carbon indicating here also that the stability of the composite is limited by selected active material and electronic additive.

In brief, this study shows that despite moisture sensitivity, LLZO:Ta garnet type can be easily used as SSE for Li-ASSB as separator and barrier to the penetration of Li dendrite and also as ionic conductive additive in the composite positive electrode for which active material and electronic conductor additive are the limiting components. Finally, to obtain a self-standing ASSB, efforts have to be driven on the selection of active materials and electronic additives.

4. Experimental Section

Materials: This report focuses on the study of the stability of LLZO:Ta while the effect of synthesis parameters is disregarded. To allow a clear separation of these parameters, and to avoid any risks of extra parameters associated to the synthesis process, all the experiments were conducted using commercial $Li_{6.4}La_3Zr_{1.4}Ta_{0.6}O_{12}$ (LLZO:Ta AmpceraTM from MSE Supplies, USA) and $LiNi_{0.8}Co_{0.1}Mn_{0.1}O_2$ (NMC from Targray).

Sintering Technique: Spark plasma sintering (SPS) technique was used for all densification/sintering experiments using a FUJI 632Lx or a Sumitomo Dr Sinter 2080 equipment. For the sintering process, graphite dies (10 mm in diameter) and graphite foils (0.2 mm disk Papyex, Mersen Group, France) were used to ensure intimate contact between powder and punches. The assembly of the mold was carried out in a glove box to avoid contact with moist air and the mold is immediately transferred to the SPS chamber and further evacuated until a 5 mPa pressure is reached. After SPS treatment, the mold was transferred and dismantled in glove box and the pellet was stored and handled in the glove box.

The compactness of the pellets was determined using the dimensions (diameter thickness) and weight of the pellets after polishing to ensure flat and parallel surfaces. The relative density was calculated by dividing the compactness of the pellets after densification by the theoretical density of LLZT (5.5 g cm^{-3}).

Characterizations: The polishing of the pellets was performed using an MECATECH 250 SPC (PRESI, France) equipment. A polishing lubricant and a high-quality polycrystalline diamond suspension water-free (NX-MET, France) were used to get clean pellets surface with low roughness.

X-ray diffraction (XRD) characterization is performed on both faces of the pellet as recovered, after polishing, and on the powder obtained after grinding. A Bruker D4 diffractometer or Bruker D8 Endeavor both using Cu Kα radiation ($\lambda = 1.5406$ Å) were used to collect diffraction patterns over the range $2\theta = 10$–$100°$ with a scanning speed of $0.02° \, s^{-1}$. Operando XRD during heating was carried out in an Anton Paar HTK1200N high-temperature chamber installed on the Bruker D8 diffractometer. The sample was heated up to 1000 °C with a heating rate of 30 °C min^{-1} and the XRD patterns were collected every 100 °C in the $2\theta = 10$–$100°$ angle range. All XRD pattern analyses were performed using the FullProf software package.[13]

The chemical composition of the samples was determined by inductively-coupled plasma emission spectroscopy (ICP-AES) using spectrometer Varian 720-ES optical emission spectrometer and estimation of the chemical formulae normalized to the La content.

Ionic conductivity was determined by electrochemical impedance spectroscopy (EIS) with an impedance analyzer MTZ-35 (Biologic, France) using a potential amplitude of 100 mV in a frequency range from 15 MHz to 1 Hz. For the EIS measurement, Au electrodes (ca 50 nm in thickness) were deposited on both sides of pellets. The pellets were placed in a controlled environment sample holder (CESH) allowing working under an argon atmosphere and connected to an intermediate temperature system (ITS) to investigate materials properties over a temperature range from -40 to 150 °C.

Supporting Information

Supporting Information is available from the Wiley Online Library or from the author.

Conflict of Interest

The authors declare no conflict of interest.

Data Availability Statement

The data that support the findings of this study are available from the corresponding author upon reasonable request.

[1] J. Janek, W. G. Zeier, *Nat. Energy* **2016**, *1*, 16141.
[2] A. Manthiram, X. Yu, S. Wang, *Nat. Mater.* **2017**, *2*, 16103.
[3] N. Kamaya, *Nat. Mater.* **2011**, *10*, 682.
[4] J.-M. Doux, *J. Mater. Chem. A* **2020**, *8*, 5049.
[5] R. Murugan, V. Thangadurai, W. Weppner, *Angew. Chem.* **2007**, *46*, 7778.
[6] V. Thangadurai, S. Narayanan, D. Pinzaru, *Chem. Soc. Rev.* **2014**, *43*, 4714.
[7] Y. Li, C.-A. Wang, H. Xie, J. Cheng, J. B. Goodenough, *Electrochem. Commun.* **2011**, *13*, 1289.
[8] Y. Wang, W. Lai, *Electrochem. Solid-State Lett.* **2012**, *15*, A68.
[9] Y. Li, J.-T. Han, C.-A. Wang, H. Xie, J. B. Goodenough, *J. Mater. Chem.* **2012**, *22*, 15357.
[10] W. Xia, *J. Am. Ceram. Soc.* **2017**, *100*, 2832.
[11] A. Sharafi, *J. Mater. Chem. A* **2017**, *5*, 13475.
[12] Y. Ren, T. Liu, Y. Shen, Y. Lin, C.-W. Nan, *J. Mater.* **2016**, *2*, 256.
[13] H. Buschmann, S. Berendts, B. Mogwitz, J. Janek, *J. Power Sources* **2012**, *206*, 236.
[14] J. Rodriguez-Carvajal, *Newsletter* **2001**, *26*, 12.
[15] J. Košir, S. Mousavihashemi, B. P. Wilson, E.-L. Rautama, T. Kallio, *Solid State Ionics* **2022**, *380*, 115943.
[16] Y. Li, J. T. Han, S. C. Vogel, C. A. Wang, *Solid State Ionics* **2015**, *269*, 57.
[17] K. P. C. Yao, *J. Electrochem. Soc.* **2013**, *160*, A824.
[18] S.-W. Baek, J.-M. Lee, T. Y. Kim, M.-S. Song, Y. Park, *J. Power Sources* **2014**, *249*, 197.
[19] H. Yamada, T. Ito, R. Hongahally Basappa, *Electrochim. Acta* **2016**, *222*, 648.
[20] N. M. Beekmans, L. Heyne, *Electrochim. Acta* **1976**, *21*, 303.
[21] N. Bonanos, P. Pissis, J. R. Macdonald, *Characterization of Materials* (Ed: E. N. Kaufmann), Hoboken **2012**, p. 114.
[22] F. Han, *Nat. Energy* **2019**, *4*, 187.
[23] Y.-T. Chen, *J. Phys. Chem. C* **2017**, *121*, 15565.